Temperature and carrier concentration dependence of Fermi arcs in moderately underdoped math xmlns="http://www.w3.org/1998/Math/MathML">mrow>msub>mi>Bi/mi>mn>2/mn>/msub>msub>mi>Sr/mi>mn>2/mn>/msub>msub>mi>CaCu/mi>mn>2/mn>/msub>msub>mi mathvariant="normal">O/mi>mrow>mn>8/mn>mo>+/mo>mi>δ/mi>/mrow>/msub>/mrow>/math> cuprate high-temperature superconductors: A joint density of states perspective

Francisco Restrepo, Junjing Zhao, Juan Carlos Campuzano, and Utpal Chatterjee

Phys. Rev. B **107**, 174519 — Published 22 May 2023

DOI: 10.1103/PhysRevB.107.174519

Temperature and carrier concentration dependence of Fermi arcs in moderately underdoped $Bi_2Sr_2CaCu_2O_{8+\delta}$ cuprate high temperature superconductors: a joint density of states perspective

Francisco Restrepo,[1] Junjing Zhao,[1] Juan Carlos Campuzano,[2] and Utpal Chatterjee[1,*]

[1]*Department of Physics, University of Virginia, Charlottesville, VA 22904*
[2]*University of Illinois at Chicago, Chicago, IL 60607*

(Dated: April 18, 2023)

Employing an autocorrelation analysis of angle resolved photoemission spectroscopy (ARPES) data, we have investigated the evolution of the joint density of states (JDOS) in the pseudogap (PG) phase of slightly underdoped $Bi_2Sr_2CaCu_2O_{8+\delta}$ (Bi2212) cuprate high temperature superconductors (HTSCs) for different temperatures (T's) and carrier concentrations (δ's). Our JDOS analysis show that the Fermi arcs expand with increasing T at a fixed δ and with increasing δ at a specific T. Qualitatively, these observations are consistent with the theoretical scenarios of the pseudogap phase being a phase incoherent d-wave superconductor, in which the Fermi arcs are described in terms of a subtle balance between temperature-dependent lifetime broadening of the single-particle excitations and the magnitude of the pairing gap.

PACS numbers:

Introduction

Central to the microscopic theory of cuprate HTSCs is unveiling the low-energy electronic excitations in the PG phase, where the electronic density of states in the vicinity of the chemical potential is suppressed even above the superconducting (SC) critical temperature (T_c)[1–11]. Theoretical models of the PG phase can be distilled into two broad categories: (i) the PG state is a precursor to the SC state[12–17], and (ii) the PG state corresponds to some broken symmetry phase that is unrelated to superconductivity[18–26].The precursor pairing and competing order parameter scenarios for the PG state are naturally related to the so-called "one-gap" and "two-gap" pictures of the energy gap below T_c, respectively. While the energy gap below T_c along the entire Fremi surface is of SC origin in the "one-gap" picture, it supposedly corresponds to different order parameters along different parts of the Fermi surface in the two-gap picture. More specifically, in the two-gap picture, the energy gap close to the node is of SC origin, while it is connected to some other type of electronic order unrelated to superconductivity near the antinode.

A series of ARPES studies have revealed that, while the electronic states in the vicinity of the zone boundary are gapped below PG temperature T^*[27,28], extended regions centered at the zone diagonals, commonly known as the Fermi arcs, are gapless[6,10,27]. In this manuscript, we have referred energy gap anywhere along the underlying Fermi surface above T_c as pseudogap. Despite detailed studies, the mechanism behind Fermi arcs remains one of the most controversial topics in the field. In the competing order parameters scenario, these Fermi arcs are pockets due to a reconstruction of the Fermi surface and they appear as arcs only because the high momentum side of the pocket has very weak intensity due to specific forms of the coherence factors. On the other hand, in some of the precursor pairing models, the Fermi arc is essentially a gapless paired state due to smearing of the energy gap induced by the broadening of the single particle spectral function[28,29].

Knowledge of how the Fermi arc length changes with T and δ can provide critical insights to distinguish between above-described contrasting scenarios of the PG phase. For instance, a T-dependent Fermi arc length will most likely be incompatible with a density-wave-driven mechanism for the PG phase. Despite a large volume of ARPES studies, the evolution of the Fermi arcs with changing T and δ is yet to be entirely settled. Some of these experiments[27,30,31] concluded Fermi arcs to be strongly T-dependent, while there are also reports[32,33] implying practically T-independent arcs. Additionally, a number of other ARPES studies have suggested possible pocket formation in the PG phase[34–40]. Similarly, results based on Scanning Tunneling Spectroscopy (STS) experiments regarding the formation of Fermi arcs are also not conclusive. For instance, while a number of STS experiments indicate competing order parameter scenario of the PG phase[41–45], there are a few other STM works[46,47] rendering support to the precursor pairing models.

ARPES investigations of the Fermi arcs, so far, have predominantly been conducted by focusing directly on the single-particle density of states (SDOS) intensity maps. In our earlier works[48,49], we demonstrated how joint density of states (JDOS) patterns can be used to identify even subtle features the of low-energy electronic excitations both in the PG and SC states. Moreover, octet model has been reported to be by and large successful in the interpretation of the Fourier transform scanning tunneling spectroscopy (FT-STS) data at least in the optimal-doped and moderately underdoped samples[48–58]. Consequently, JDOS analysis can potentially offer a bridge between real- and momentum-space spectroscopic techniques. There are, however, studies[59–61] which go beyond the Octet model towards the decsription of FT-STS patterns. Moreover, some of the JDOS studies[58]

reported discrepancy between gap symmetry obtained from ARPES and STS data, especially in the underdoped regime. Here, our plan is to exploit the unique capability of the autocorrelation analysis in terms of unveiling subtle spectral features from the ARPES data, that may not be easily discernible from the SDOS maps, to interrogate T- and δ-dependence of the Fermi arc contours.

The peaks of a constant energy (ω) JDOS map relate to the momentum separations ($\mathbf{q}$'s) between regions with high spectral intensities of the SDOS map at that fixed value of ω[48–53]. As has been elaborated in our earlier works[48,49], the autocorrelation function (defined in Eq. 1) of an SDOS map at a fixed ω can be mapped to the JDOS map at the corresponding ω. These works have also demonstrated that the peaks of a JDOS map (for $\omega <$ antinodal energy gap Δ_0) at a constant ω relate predominantly to the $\mathbf{q}$'s separating edges of the SDOS map at that specific ω both in the PG and SC states. Consequently, the variation of $|\mathbf{q}|$ associated with a specific peak of a constant ω JDOS map with changing T and δ will capture the associated modifications in the Fermi arc lengths. In this work, we mainly consider $\mathbf{q}$ vectors along the Cu-O bond direction, i.e., $\mathbf{q}_1$ and $\mathbf{q}_5$ as referred in the octet model[51–53].

Our findings are as follows: $|\mathbf{q}_1|$ gets shorter and $|\mathbf{q}_5|$ gets longer as T (δ) is increased at a fixed δ (T). Collectively, these will imply that the extensions of the Fermi arc contours in the PG phase depend upon T and δ—more specifically, the Fermi arcs expand with increasing T (δ) at a given δ (T). By comparing with the JDOS patterns simulated from a model of disordered d-wave superconductor, we further show that he subtle balance between T-dependent spectral broadening Γ above T_c and the strength of pairing correlations quantified by Δ_0, can provide a possible phenomenology of the Fermi arcs at least in optimally doped and moderately underdoped cuprate HTSCs.

Results

Our present work is based on ARPES data from two underdoped Bi2212 single crystals — one of them is with $T_c \sim 80$ K (labeled UD80) and the other with $T_c \sim 85$ K (labeled UD85)– and a thin film sample with $T_c \sim 67$ K (labeled UD67). The results of our ARPES experiments and simulations will be organized as follows. In Sec. A, we will briefly discuss general ideas on the autocorrelation analysis and the relation between autocorrelation and JDOS maps. The experimental data on T and δ dependence of the JDOS of underdoped Bi2212 cuprate HTSCs will be described in Sec. B and C, while we will make an effort to rationalize these results using a broadened d-wave picture of the PG phase in Sec. D. Finally, we will interrogate the evolution of the length of the Fermi arcs as a function of δ and T from that of the autocorrelation features as a function of δ and T.

A. Connection between Autocorrelation and JDOS patterns

A constant energy ARPES intensity map represents ARPES data $I(k_x, k_y, \omega)$, where the electronic energy ω is referenced to the chemical potential, and k_x, k_y are the x- and y-components of the in-plane momentum vector $\mathbf{k}$. Such an intensity map describes the $\mathbf{k}$-resolved SDOS at that fixed value of ω. It should be noted that we haven't factored out the effect of Fermi function from these maps. We, however, would like to note that this doesn't cause any issue to the current analysis since we will only consider elastic autocorrelations. Fig. 1a displays the SDOS map for the UD80 sample in the SC state (T=40 K) for ω=0 meV. It shows characteristic banana-shaped contours centered at the nodes and with strongly peaked intensities close to the banana tips due to large value of the curvature of the dispersion, i.e., $\left|\frac{1}{\Delta_{\mathbf{k}}\ \omega(\mathbf{k})}\right|$. These contours expand with increasing $|\omega|$ due to d-wave SC energy gap and strong momentum anisotropy of the underlying electronic structure in cuprate HTSCs. A one-to-one mapping between the autocorrelation function $C(\mathbf{q}, \omega)$ and the momentum-resolved JDOS has been elaborated in our earlier works[48,49], where $C(\mathbf{q}, \omega)$ is defined as follows:

$$C(\mathbf{q}, \omega) = \sum_{k_x, k_y} I(k_x, k_y, \omega) I(k_x + q_x, k_y + q_y, \omega), \quad (1)$$

such that $\mathbf{q} = (q_x, q_y)$ is the momentum transfer and the momentum sum is over the first Brillouin zone. Because of the specific shape of the SDOS maps as described above, eight $\mathbf{q}$ vectors $\mathbf{q}_i$ ($i = 1, 2, \cdots, 8$) (Fig. 1a) dominate the $C(\mathbf{q}, \omega)$ intensity maps at each ω for $|\omega| \leq \Delta_0$.Two of these vectors,namely q_8 and q_4, are identical due to the underlying symmetry of the system. In Fig. 1b, we show $C(\mathbf{q}, \omega)$ for the UD80 sample in the SC state. Each $\mathbf{q}_i$ ($i = 1, 2, \cdots, 7$) as in the octet model can be identified in Fig. 1b, but here we only point to a few of them for visual clarity.

B. Temperature-dependent JDOS patterns in the PG state

Temperature-dependent Fermi arcs and corresponding JDOS maps in the PG state of the UD80 sample are displayed in Figs. 1c–1f, where Figs. 1c–1d correspond to T = 110 K and Figs.1e–1f to T=200 K, respectively. In this connection, we note that the SDOS map at $\omega = 0$ meV at a given $T > T_c$, represents the Fermi arc at that specific T. A comparison of Figs. 1d, 1f with Fig. 1b highlights similarity between JDOS patterns in the PG and SC states. This is consistent with our finding in our earlier work[48], where we showed that at temperatures both below and above T_c, the peaks of a JDOS map at a fixed ω of can be tied to the $\mathbf{q}$'s separating edges of the

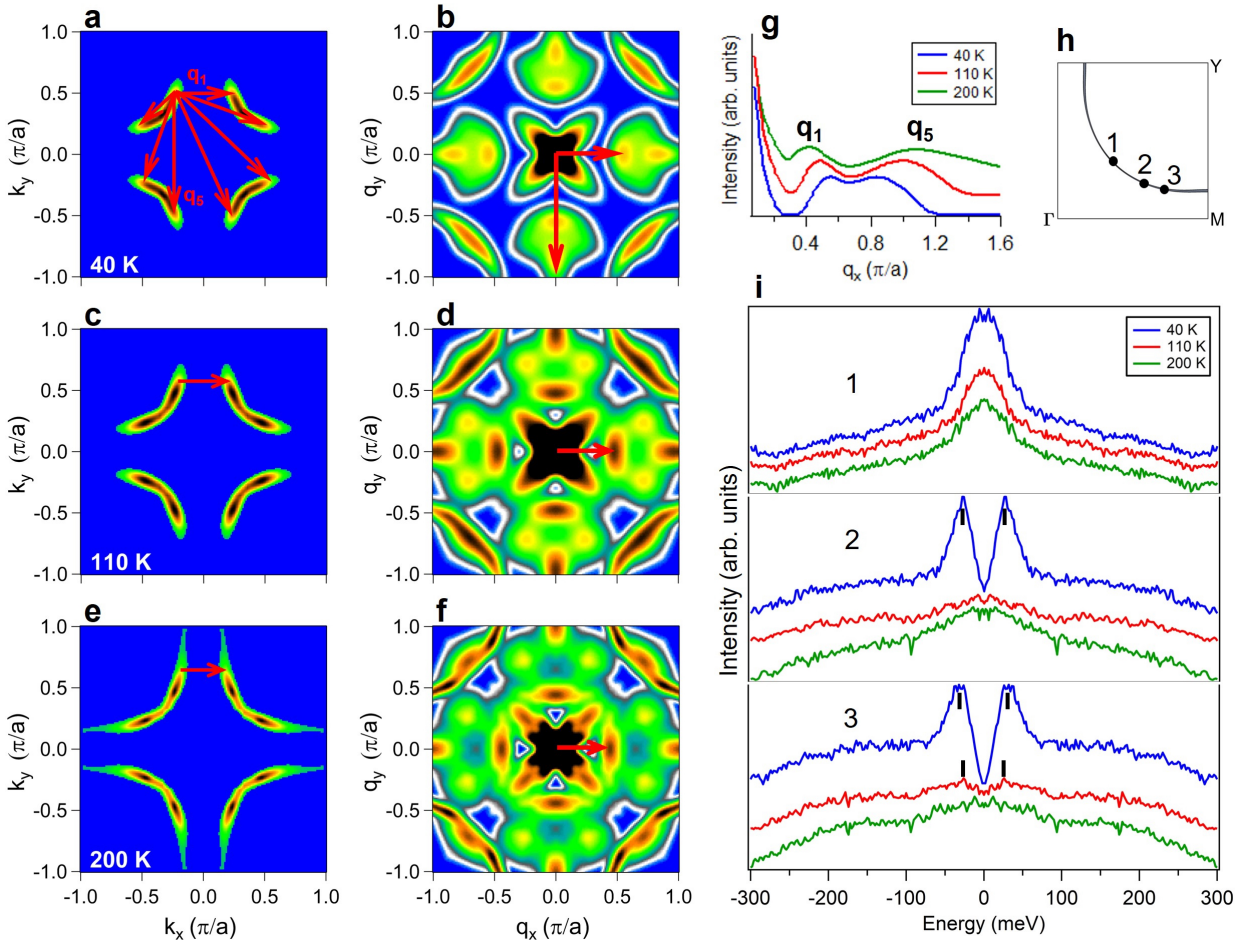

FIG. 1: Temperature-dependent Fermi arcs, autocorrelation maps, and symmetrized EDCs at various Fermi momenta for the UD80 sample. SDOS map and the corresponding JDOS map at ω =0 meV for T=40K are shown in (a) and (b), respectively. (c), (d) same as (a), (b) but with T = 110 K. (e), (f) same as (a), (b) but with T = 200 K. Variois $\mathbf{q}$'s as per Octet model are shown in (a). (g) JDOS line cuts in the (q_x, 0) direction at ω=0 meV forthe UD80 sample at 40 K (blue), 110 K (red), and 200 K (green). Curves are offset for visual clarity. (h) Approximate locations of the Fermi momenta associated with the symmetrized EDCs plotted in (i) are shown on the schematic plot of the Fermi surface.

single-particle density of states (SDOS) intensity map at that specific ω—in other words, there is no qualitative difference between the JDOS patterns below and above T_c. We analyze the evolution of the $\mathbf{q}$ vectors with T in the PG state by concentrating specifically on $\mathbf{q}_1$ and $\mathbf{q}_5$. To this end, we plot the JDOS line cuts along the (q_x, 0) direction for ω = 0 meV as shown in Fig. 1g. Evidently, with increasing T, $|\mathbf{q}_1|$ becomes shorter and $|\mathbf{q}_5|$ becomes longer, indicating a lengthening of the Fermi arc in the PG state with increasing T. We would like to point out that the momentum separation ($\Delta q_{\omega=0}$) between the peaks associated with $\mathbf{q}_1$ and $\mathbf{q}_5$ at ω = 0 mev is finite below T_c. This may seem to represent a Fermi arc even below T_c since the presence of a node in the superconducting gap should have been manisfeted as $\Delta q_{\omega=0} = 0$ for $\omega = 0$ We believe that this apparent inconsistency is predominantly a result of finite energy resolution, which we further examine using temperature-dependent measurements below T_c in Fig. 2.

The above observations regarding the T dependence of the Fermi arcs can also be corroborated from ARPES energy distribution curves (EDCs) (Fig. 1i), where an EDC is a plot of $I(k_x, k_y, \omega)$ as a function of ω at a specific momentum location (k_x, k_y). For brevity, we display EDCs only at three points on the Fermi surface as indicated in Fig. 1h. We have symmetrized the EDCs to approximately remove the effect of the Fermi function from the data. Point 1 corresponds to the node and the EDC at this point is expectedly gapless at each temperature, which is evident from the presence of a peak at ω = 0 meV. At point 2, in between the node (point 1) and the antinode, the spectrum at 40 K is gapped as expected from the fact that d-wave superconducting energy gap is finite away from the node, while the data at higher temperatures are ungapped. The presence of an energy gap in the SC state is revealed by the double-peak structure of the symmetrized EDC at 40 K. This implies that the gapless point node in the SC state turns into an extended

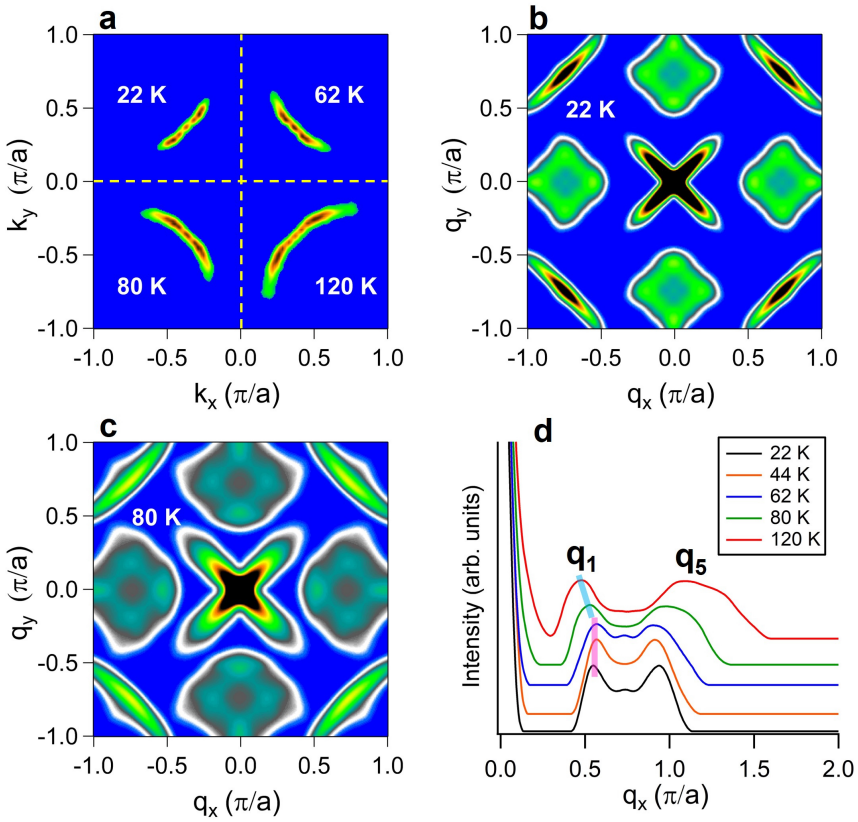

FIG. 2: Temperature evolution of the SDOS and JDOS intensity maps for the UD67 sample. (a) SDOS map (plotted only in a single quadrant for visual clarity) at ω=0 meV for the UD67 sample at 22 K, 62 K, 80 K, and 120 K. JDOS patterns at (b) 22 K and (c) 80 K. (d) Temperature-dependent cuts through the JDOS patterns at ω=0 meV along the (q_x, 0) direction.

gapless region, i.e., a Fermi arc, at 110 K and this Fermi arc persists at higher temperatures. Finally, at point 3, between point 2 and the antinode, the spectra at 40 K and 110 K are gapped, while it is ungapped at 200 K. In other words, point 3 lies beyond the arc at 110 K, but within the Fermi arc at 200 K. This is consistent with the JDOS analysis, in which the Fermi arcs are found to become progressively larger with increasing temperature in the PG state. In several published works, the lengthening of the Fermi arc with increasing T in the PG state has been interpreted via T-dependent enhancement in spectral broadening (Γ)[28,29,62]. This can be realized from Fig.1i, in which a monotonic increase in Γ of the symmetrized EDCs with increasing T can be easily recognized even without a quantitative analysis.

We present a similar data analysis for the UD67 sample in Fig. 2. In addition to providing an opportunity to compare with the results presented in Fig. 1, the data from the UD67 sample as a function of temperature through T_c also helps us to examine the impact of energy resolution on JDOS analyis. The effect of energy resolution is expected to impact results especially at low temperatures (particularly below T_c), where the spectral features are quite sharp. Fig. 2d presentes data similar to that in Fig. 1g. As in Fig. 1g, $\Delta q_{\omega=0}$ here is also finite even below T_c. However, $\Delta q_{\omega=0}$ as a function of temperature below T_c remains almost the same. But it increases discontinuously as the temperature is increased slightly above T_c and increases monotonically with further increase in temperature. Therefore, the temperature dependence of $\Delta q_{\omega=0}$ above T_c is qualitatively different from that below T_c. In other words, the appearance of a Fermi arc below T_c is predominantly an energy resolution issue, while it is an intrinsic feature above T_c. In this context, the presence of a node in the superconducting gap is a characteristic feature of d-wave order paraemeter in cuprate HTSCs, which has been established via different experimental probes at least in the doping range of the current study. In short, the results from the UD67 and UD80 samples in the PG state are overall consistent with each other–(i) The JDOS patterns below and above T_c are qualittaively same, and (ii) $\Delta q_{\omega=0} = 0$ grows with increasing temperature (Fig. 2d and Fig. 1g).

C. Carrier Concentration-dependent JDOS patterns

We now explore the evolution of the JDOS patterns with changing δ at a fixed T. To this end, we compare

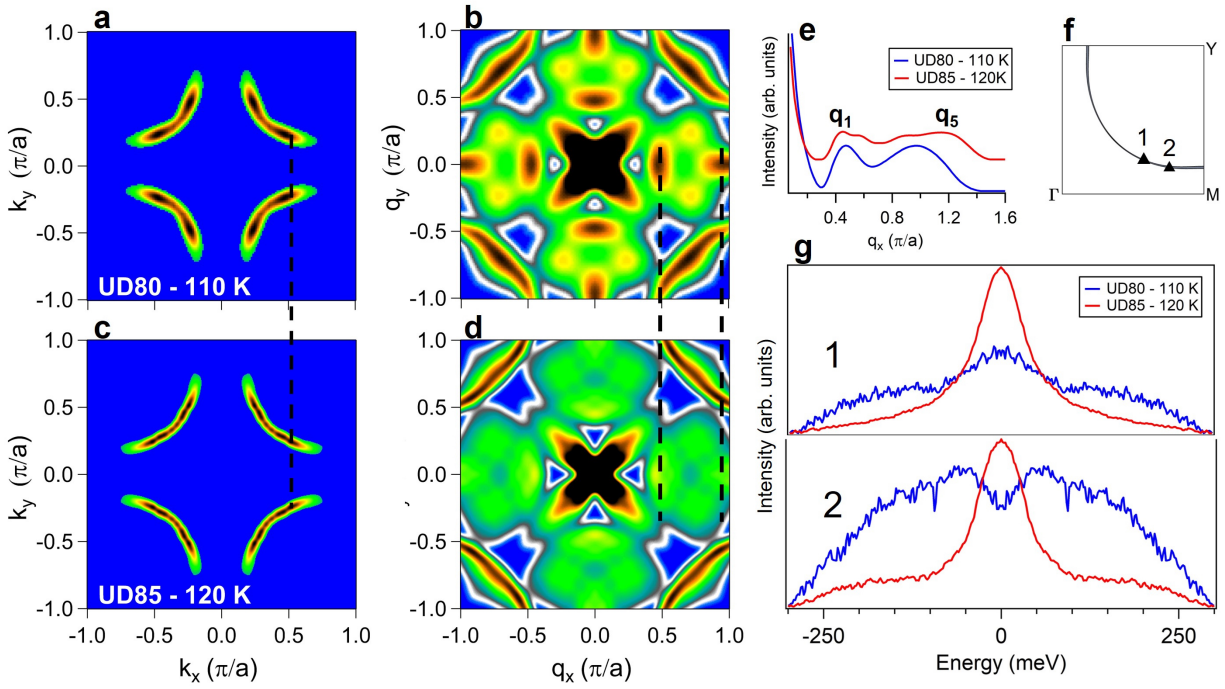

FIG. 3: Carrier concentration dependence of Fermi arcs based on JDOS maps. (a) Fermi arc, i.e., SDOS map at $\omega = 0$ meV, for the UD80 sample at 110 K. (b) JDOS map obtained from autocorrelation of the SDOS map in (a). (c), (d) Same as (a), (b) but for the UD85 sample at 120 K. (e) JDOS line cuts in the (q_x, 0) direction for the UD80 (blue) and UD85 samples (red). (f) Approximate momentum coordinates of the EDCs plotted in (g) are shown on the schematic plot of the Fermi surface. (g) Symmetrized EDCs from the UD80 (blue) and UD85 (red) samples at points straddling the Fermi arc tip of the UD80 sample (black triangles 1 and 2 in (f), respectively).

data from the UD80 and UD85 samples at $T \sim 110$ K in Fig. 3. Fig. 3a displays the Fermi arc, i.e., SDOS map at $\omega = 0$ meV from the UD80 sample at $T = 110$ K, while Fig. 3b shows the corresponding JDOS map. Likewise, Figs. 3c, d show the Fermi arc and JDOS maps of the UD85 sample at 120 K. The two vertical dashed lines in Figs. 3b, d compare $|\mathbf{q}_1|$ and $|\mathbf{q}_5|$ of these two samples at $\omega = 0$ meV. In comparison with the UD80 sample, $|\mathbf{q}_1|$ and $|\mathbf{q}_5|$ for the UD85 sample are smaller and larger, respectively. This is more clearly visible in the plots of the line cuts of $C(\mathbf{q}, \omega)$ maps in Fig. 3e along (q_x, 0) direction, i.e., along the bond direction. It can be easily verified that $|\mathbf{q}_1|$ ($|\mathbf{q}_5|$) of UD85 sample is smaller (larger) compared to that of the UD80 sample. We would like to point out that the observed change in $|\mathbf{q}_5|$ is more prominent compared to that of $|\mathbf{q}_1|$ because of the topology of the SDOS maps. The dashed vertical line in Figs. 3a, c indicates that a similar conclusion, i.e., increasing Fermi arc length with increasing δ at a fixed T, can also be reached from a direct comparison of the SDOS maps of the UD80 andUD85 samples.

To elucidate the origin of this δ-dependence, we now compare the symmetrized EDCs from the UD80 and UD85 samples at similar temperatures (110 and 120 K, respectively), at the two points indicated in Fig. 3f. At point 1, closer to the node, the spectra are gapless, meaning that point 1 resides on the Fermi arc of both samples. Moreover, just from visual inspection, it can be seen that the EDC from the UD80 sample is broader than that from the UD85 sample. At point 2, the EDC from the UD85 sample remains gapless, while the EDC from the UD80 sample is gapped. In other words, point 2 resides outside the Fermi arc of UD80. This is consistent with the fact that the arc is longer for the UD85 sample. It is worth noting that unlike in Fig. 3, the lengthening of the Fermi arc here cannot be attributed to an increase in Γ because the spectra from the UD80 sample is broader compared to that from the UD85 sample (Fig. 3g). In other words, the Fermi arc lengths in samples with different δ cannot be described by Γ alone, the magnitude of Δ_0 also needs to be included—Δ_0 of UD85 sample is smaller than that of the UD80 sample. More precisely, the Fermi arc length depends on the relative magnitude of Γ with respect to Δ_0, which we will examine in Sec. D using a life-time broadened d-wave model[28,29] for the PG phase. In passing, we would like to comment that it is not straightforward to reconcile the observation of temperature-dependent Fermi arc length with completing order parameter scenarios, rather it appears to be naturally consistent with an incoherent SC order parameter interpretation for the PG state in which the Fermi arc originates due to smearing of the pairing gap induced by spectral broadening. We elaborate this in Section. D

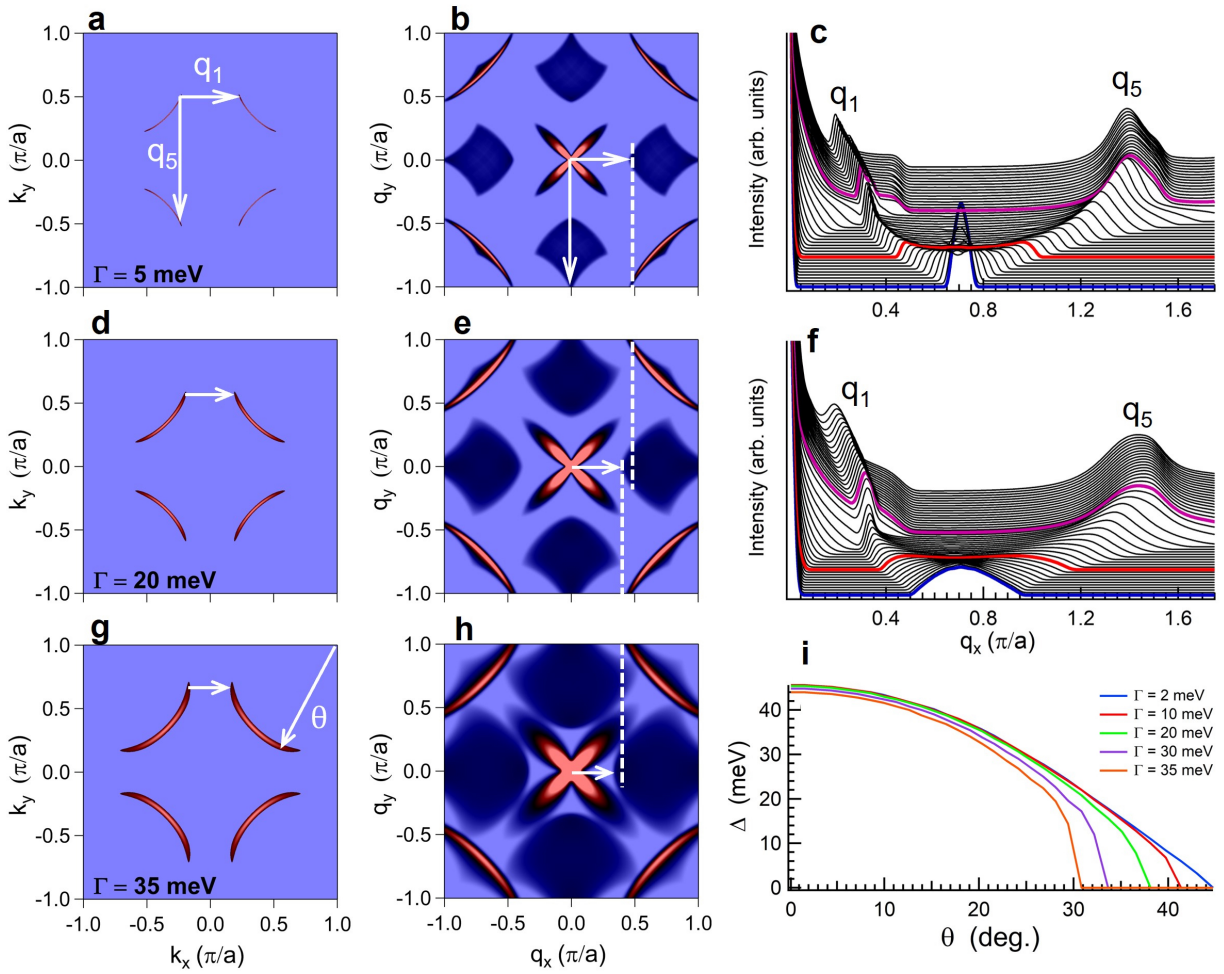

FIG. 4: Simulated SDOS and corresponding JDOS maps as a function of the broadening parameter Γ in the broadened, d-wave model. (a), (b) Calculated SDOS at and corresponding autocorrelation map for Γ = 5 meV. (c) Cuts through the autocorrealtion map in (b) along the direction (q_x, 0) for eneries in the range (0, 80) meV, separated by 2 meV intervals. (d)–(f) Same as (a)–(c), but with Γ = 20 meV. (g), (h) Same as (a), (b), but with Γ = 35 meV. (i) Spectral gap versus Fermi surface angle for five different values of Γ. All intensity maps in (a), (b), (d), (e), (g), and (h) were calculated at ω = -20 meV. In (c), the blue, red, and purple curves correspond to $|\omega|$ = 0, 20 and 50 meV, respectively. In (f), the blue, red, and purple curves correspond to $|\omega|$ = 0, 20 and 46 meV, respectively. Throughout this figure, Δ_0 = 50 meV.

D. Simulated JDOS patterns based on a broadened d-wave model

Here, we will discuss our results in the context of a broadened, d-wave model of the PG phase. We will consider the following Green's function[28]:

$$G^{-1}_{\mathbf{k},\omega} = \omega - \epsilon_{\mathbf{k}} = i\Gamma - \frac{\Delta^2_{\mathbf{k}}}{\omega + \epsilon_{\mathbf{k}} + i\Gamma}, \qquad (2)$$

where $\Delta_{\mathbf{k}} = \frac{\Delta_0}{2}(\cos k_x - \cos k_y)$ is the d-wave gap, $\epsilon_{\mathbf{k}}$ is a tight binding fit to the Bi2212 dispersion[57], and Γ represents the effective broadening of the single-particle excitations. In a more rigorous approach, we should have separately considered intrinsic broadening and thermal broadening. Our aim, however, here is to adopt a minimal model and thus, we have used a single broadening parameter Γ to take both into account. Typically, a very small value of Γ, representing intrinsic broadening, is used to describe the SC state with no disorder. We note that the nodal structure will vanish for any finite value of Γ and thus, an arc will emerge even in the SC state. This is clearly an artifact since there is no Fermi arc in the SC state at least in the moderately underdoped regime. We, however, would like to emphasize that this is not an issue for the current analysis since we are interested in the PG state—in particular, our focus is to observe what happens to the extent of the gapless regions along the Fermi surface with increasing Γ. Nevertheless, the arc-like region in the SC state can be made infinitesimally small by selecting a very small value of Γ. We noticed that for the parameters used in the current case, 2 meV is a reasonable magnitude of Γ so as to ensure

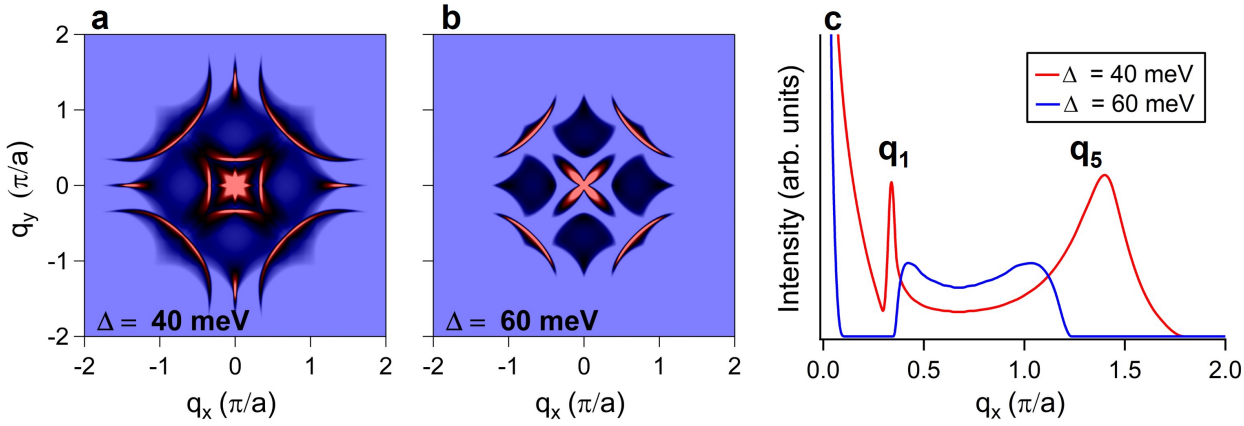

FIG. 5: Effect of Δ_0 on JDOS maps in the broadened d-wave model. (a), (b) JDOS patterns obtained from autocorrelation of Eq. 2 with Δ_0 = 40 meV and 60 meV, respectively. (c) Horizontal cuts through (a) and (b) in the (q_x, 0) direction. In all panels, Γ = 20 meV and the ω = -30 meV.

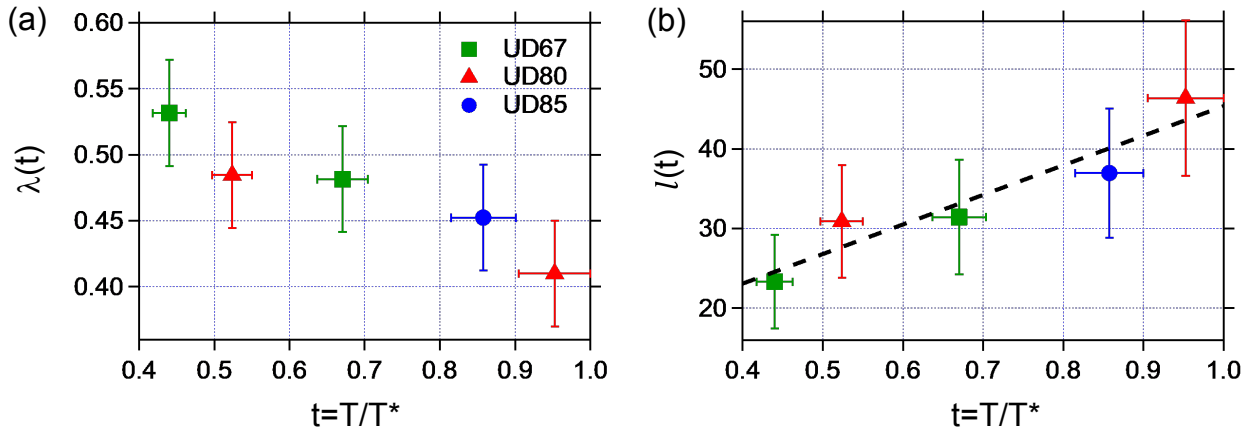

FIG. 6: Dependence of Fermi arc length on reduced temperature t. (a) and (b) show the plots of of $\lambda(t)$ and $l(t)$, respectively. Blue circle correspond to the UD85 sample. Red triangles represent to the UD80 sample, while Green squares to the UD67 sample. The black dashed line is a linear fit to the data points representing $l(t)$ in (b).

that there is no discernable Fermi arc in the SC state.

Intensity plots of $(-\frac{1}{\pi}$ Im $G_{\mathbf{k},\omega})$ as a function of k_x and k_y at a fixed ω represent $\mathbf{k}$-resolved SDOS maps at that specific value of ω. We show the SDOS map at ω = -20 meV for Γ = 5 meV in Fig. 4a and the corresponding JDOS map in Fig. 4b. The dispersion of $|\mathbf{q}_1|$ and $|\mathbf{q}_5|$with $|\omega|$ is shown in Fig. 4c, where we plot cuts through the $C(\mathbf{q},\omega)$ map along the (q_x, 0) direction for various values of $|\omega|$. The bottom, blue curve (at ω = 0 meV) is characterized by a broad peak instead of two separate peaks. This is due to the fact that the spectral broadening makes it difficult to resolve the peaks associated with $\mathbf{q}_1$ and $\mathbf{q}_5$. As the contours in the SDOS maps expand with increasing $|\omega|$, peaks corresponding to $\mathbf{q}_1$ and $\mathbf{q}_5$ begin to disperse away from each other. The purple curve in Fig. 4c corresponds to $|\omega| \sim \Delta_0$, beyond which the dispersion of the $\mathbf{q}$ vectors is dictated by the underlying band dispersion. As Γ is increased from 5 to 20 meV the SDOS contours become longer, as can be realized from a comparison of Figs. 4a and 4d. Expectedly, the autocorrelation features become blurrier with increasing Γ. Cuts through the $C(\mathbf{q},\omega)$ map along the (q_x, 0) direction for various values of $|\omega|$ in the case of Γ = 20 meV are presented in Fig. 4f. As in Fig. 4c, the separation of the peaks associated with $\mathbf{q}_1$ and $\mathbf{q}_5$ at ω = 0 meV (blue curve at bottom) is not visible due to spectral broadening. Therefore, we compare the arc length by focusing on the line cuts away from ω = 0 meV so that the separation between peaks associated with $\mathbf{q}_1$ and $\mathbf{q}_5$ is clearly observable. Apparently, ω = -20 meV works well for this purpose as in Fig. 4c and Fig. 4f. The trend observed by increasing Γ from 5 meV to 20 meV continues as Γ is further increased to 35 meV (Figs. 4g, h). Fig. 4i shows the dependence of the energy gap on the Fermi surface angle (Fig. 4g) for different broadening values. The gap values were obtained by measuring the peak-to-peak distance in the Energy Distribution Curves (EDCs) on the Fermi surface[10]. Evidently, increasing Γ

leads to larger Fermi arcs.

To explore how Fermi arc length depends on Δ_0 in this model, we fix the broadening parameter Γ and vary Δ_0 as shown in Fig. 5. We plot the JDOS maps with Γ = 20 meV at ω = -30 meV, where peaks associated with $\mathbf{q}_1$ and $\mathbf{q}_5$ are well separated. Fig. 5a and Fig. 5b show the JDOS patterns for $\Delta_0 = 40$ and 60 meV, respectively. The main qualitative difference between the two patterns is the size of the four petal-shaped features surrounding the center from the q_x and q_y directions. These are evidently larger for the smaller gap. This, in turn, means that $|\mathbf{q}_1|$ ($|\mathbf{q}_5|$) becomes shorter (longer) with decreasing Δ_0 at a fixed value of Γ. This is can be easily verfied from the plot of the cut along the $(q_x, 0)$ direction through the JDOS maps in Fig. 5a, b. In Fig. 5c, we compare these cuts, which clearly show that $|\mathbf{q}_1|$ becomes shorter with decreasing Δ_0, while $|\mathbf{q}_5|$ becomes longer. Therefore, the Fermi arc contours must be shrinking with decreasing Δ_0. Thus, from the broadened d-wave model for the Fermi arcs, we conclude that the arc length depends on the balance between Δ_0 and Γ.

E. Temperature dependence of Fermi arc length from JDOS analysis:

In one of our previous works[30], we showed that the length of the Fermi arcs over an extended region of the PG phase of Bi2212 HTSCs can be well approximated by a linear function of the reduced temperature t, where t is the ratio of the sample temperature T to T^*. It is instructive to explore whether such t dependence of the Fermi arc lengths can be detected from the temperature-dependent autocorrelation data. The present analysis has access to five data points above T_c: two for the UD80 sample, one for the UD85 sample, and two for the UD67 thin film. We plot $\lambda \equiv |\mathbf{q}_1|_{\omega=0}$ for these data points as a function of t in Fig. 6a. Note that we chose $|\mathbf{q}_1|$ instead of $|\mathbf{q}_5|$ because the peak structure of $\mathbf{q}_5$ is substantially broader. The uncertainties in $|\mathbf{q}_1|$ come from the peak widths in the horizontal cuts through the JDOS maps, while the uncertainties in t come from the error bar in determining T^*. As to the estimation of T^*, we employed two different methods. In the first method, we considered the filling up of spectral gap at the antinode using the following: $L = 1 - \left(\frac{I(\omega=0)}{I(\omega=-\Delta_0)}\right)$, where $I(\omega = 0)$ and $I(\omega = -\Delta_0)$ are the ARPES intensities (after symmetrization) at the antinode for $\omega = 0$ and $\omega = -\Delta_0$, respectively. A linear extrapolation of L to zero provides an approximation for T^*. In the second method, we used the empirical relation between the antinodal energy gap Δ_0 and T^* as presented in Fig. 4b of[63]. Both methods yielded T^* values in the range of 210-230 K for the UD80 sample. A single data point above T_c is available for the the UD85 sample and consequently, we only employed the second method, yielding T^* ~140 K. For the UD67 sample, the L-analysis gave the estimated T^* ~170-190K. As can be seen from Fig. 6a, there is a monotonic decrease of λ with increasing t, which in turn implies a monotonic increase in Fermi arc length (l) with t. This is indeed consistent with our earlier studies on the detailed doping and temperature dependennce of l. For a direct visualization, we have estimated $l(t)$ from $\lambda(t)$ and plotted it in Fig. 6b. The details of the method adopted for this estimation is provided in section 2 of the supplementary section [64]. As shown in Fig. 6b, $l(t)$ to the first approximation can be described by a linear function of t—$l(t)$ seems to fit well with a functional form $a + b(t)$. Most likely, the a term in $l(t)$ is an effect of finite energy resolution. A robust functional form of $l(t)$ from the JDOS analysis would indeed require substantially larger dataset, particularly from the PG phase in the lightly-doped region of the phase diagram.

Conclusions

In conclusion, our JDOS studies on samples in the PG state reveal that the Fermi arc lengths are T- and δ-dependent. Using simulations, based on a broadened d-wave superconducting picture for the PG phase, we show that the above results can potentially be interpreted as follows: (a) the increase/decrease in Fermi arc length at a fixed δ with increasing/decreasing T is controlled by $\Gamma(T)$; and (b) the variation of the Fermi arc length at a fixed T as a function of δ can be interpreted in terms of a balance between $\Gamma(T)$ above T_c and the strength of the pairing correlations, quantified by the gap Δ_0.

Methods

The ARPES data used in this work were collected from single crystal samples of $Bi_2Sr_2CaCu_2O_{8+\delta}$ cuprate HTSCs. Data were collected using 22 eV photon energy. During data collection, the Cu-O bond direction was kept parallel to the photon polarization. The samples were cleaved *in-situ* at a base pressure of 5×10^{-11} Torr. Measurements were carried out at the PGM beamline of the Synchrotron Radiation Center in Madison, Wisconsin. The energy resolution was ~15 meV for the UD85 dataset and ~25 meV for the UD80 dataset, and the momentum resolution was ~0.005 Å^{-1} along the multiplexing direction of the detector, and ~0.025 Å^{-1} along the perpendicular direction.The data were taken in the quadrant of the Brillouin zone which contains the "Y" symmetry point to minimize superlattice effects. The details of the data analysis procedures to construct the SDOS maps in the whole Brillouin zone was detailed in our previous work[48]. For every binding energy ω_0, ARPES intensities satisfying the condition $I(\mathbf{k}, \omega_0) < \alpha \cdot \max[I(\mathbf{k}, \omega_0)]$ were zeroed, to eliminate superlattice contributions and increase the contrast of autocorrelation features. To allow for meaningful comparisons, the parameter α was set to 0.4 for all autocorrelation calculations from ARPES data. For the same reason, all data were normalized at

300 meV binding energy. For the model calculations of Fig. 3, we used $\alpha = 0.6$, to eliminate the signal from backfolded bands due to the Bogoliubov coherence factors.

A 2-D moving average smoothing (window size: 5^2 pixels) was applied to the intensity maps. Aside from normalization and second-order light subtraction, the EDCs presented in Figs. 1 and 3 are raw data, that is, no thresholding nor background subtraction was performed.

Acknowledgements

U.C. acknowledges support from the National Science Foundation under grant number DMREF DMR-1629237.

Conflicts of interest

The authors acknowledge no conflict to disclose.

Data availability statement

The data that support the findings of this study are available from the corresponding authors upon reasonable request.

* uc5j@virginia.edu (U.C.)

[1] W.W. Warren, R.E. Walstedt, G.F. Brennert, R.J. Cava, R. Tycko, R.F. Bell, and G. Dabbagh, Physical Review Letters **62**, 1193 (1989).
[2] H. Alloul, T. Ohno, and P. Mendels, Physical Review Letters **63**, 1700 (1989).
[3] B. Bucher, P. Steiner, J. Karpinski, E. Kaldis, and P. Wachter, Phys. Rev. Lett. **70**, 2012 (1993).
[4] C.C. Homes, T. Timusk, R. Liang, D.A. Bonn, and W.N. Hardy, Physical Review Letters **71**, 1645 (1993).
[5] T. Ito, K. Takenaka, and S. Uchida, Phys. Rev. Lett. **70**, 3995 (1993).
[6] H. Ding, T. Yokoya, J.C. Campuzano, T. Takahashi, M. Randeria, M.R. Norman, T. Mochiku, K. Kadowaki, and J. Giapintzakis, Nature **382**, 51 (1996).
[7] A.V. Puchkov, D.N. Basov, and T. Timusk, J. Phys.: Condens. Matter **8**, 10049 (1996).
[8] A.G. Loeser, Z.-X. Shen, D.S. Dessau, D.S. Marshall, C.H. Park, P. Fournier, and A. Kapitulnik, Science **273**, 325 (1996).
[9] D.S. Marshall, D.S. Dessau, A.G. Loeser, C.-H. Park, A.Y. Matsuura, J.N. Eckstein, I. Bozovic, P. Fournier, A. Kapitulnik, W.E. Spicer, and Z.-X. Shen, Phys. Rev. Lett. **76**, 4841 (1996).
[10] M.R. Norman, H. Ding, M. Randeria, J.C. Campuzano, T. Yokoya, T. Takeuchi, T. Takahashi, T. Mochiku, K. Kadowaki, P. Guptasarma, and D.G. Hinks, Nature **392**, 157 (1998).
[11] T. Timusk and B. Statt, Rep. Prog. Phys. **62**, 61 (1999).
[12] M. Randeria, N. Trivedi, A. Moreo, and R.T. Scalettar, Phys. Rev. Lett. **69**, 2001 (1992).
[13] V.J. Emery and S.A. Kivelson, Nature **374**, 434 (1995).
[14] E.W. Carlson, S.A. Kivelson, V.J. Emery, and E. Manousakis, Phys. Rev. Lett. **83**, 612 (1999).
[15] H.-J. Kwon, A.T. Dorsey, and P.J. Hirschfeld, Phys. Rev. Lett. **86**, 3875 (2001).
[16] E. Berg and E. Altman, Phys. Rev. Lett. **99**, 247001 (2007).
[17] P.A. Lee, N. Nagaosa, and X.-G. Wen, Reviews of Modern Physics **78**, 17 (2006).
[18] S.A. Kivelson, E. Fradkin, and V.J. Emery, Nature **393**, 550 (1998).
[19] V.J. Emery, S.A. Kivelson, and J.M. Tranquada, Proceedings of the National Academy of Sciences **96**, 8814 (1999).
[20] M. Vojta and S. Sachdev, Phys. Rev. Lett. **83**, 3916 (1999).
[21] S. Chakravarty, R.B. Laughlin, D.K. Morr, and C. Nayak, Phys. Rev. B **63**, 094503 (2001).
[22] S.A. Kivelson, I.P. Bindloss, E. Fradkin, V. Oganesyan, J.M. Tranquada, A. Kapitulnik, and C. Howald, Rev. Mod. Phys. **75**, 1201 (2003).
[23] C.M. Varma, Phys. Rev. B **73**, 155113 (2006).
[24] C. Honerkamp, H.C. Fu, and D.-H. Lee, Phys. Rev. B **75**, 014503 (2007).
[25] M. Vojta, Advances in Physics **58**, 699 (2009).
[26] E. Fradkin, S.A. Kivelson, M.J. Lawler, J.P. Eisenstein, and A.P. Mackenzie, Annual Review of Condensed Matter Physics **1**, 153 (2010).
[27] A. Kanigel, U. Chatterjee, M. Randeria, M.R. Norman, S. Souma, M. Shi, Z.Z. Li, H. Raffy, and J.C. Campuzano, Phys. Rev. Lett. **99**, 157001 (2007).
[28] M.R. Norman, A. Kanigel, M. Randeria, U. Chatterjee, and J.C. Campuzano, Phys. Rev. B **76**, 174501 (2007).
[29] A.V. Chubukov, M.R. Norman, A.J. Millis, and E. Abrahams, Phys. Rev. B **76**, 180501 (2007).
[30] A. Kanigel, M.R. Norman, M. Randeria, U. Chatterjee, S. Souma, A. Kaminski, H.M. Fretwell, S. Rosenkranz, M. Shi, T. Sato, T. Takahashi, Z.Z. Li, H. Raffy, K. Kadowaki, D. Hinks, L. Ozyuzer, and J.C. Campuzano, Nat. Phys. **2**, 447 (2006).
[31] K. Nakayama, T. Sato, Y. Sekiba, K. Terashima, P. Richard, T. Takahashi, K. Kudo, N. Okumura, T. Sasaki, and N. Kobayashi, Phys. Rev. Lett. **102**, 227006 (2009).
[32] R. Comin, A. Frano, M.M. Yee, Y. Yoshida, H. Eisaki, E. Schierle, E. Weschke, R. Sutarto, F. He, A. Soumyanarayanan, Y. He, M. Le Tacon, I.S. Elfimov, J.E. Hoffman, G.A. Sawatzky, B. Keimer, and A. Damascelli, Science **343**, 390 (2014).
[33] T. Kondo, A.D. Palczewski, Y. Hamaya, T. Takeuchi, J.S. Wen, Z.J. Xu, G. Gu, and A. Kaminski, Phys. Rev. Lett. **111**, 157003 (2013).
[34] H.-B. Yang, J.D. Rameau, P.D. Johnson, T. Valla, A. Tsvelik, and G.D. Gu, Nature **456**, 77 (2008).
[35] J. Meng, G. Liu, W. Zhang, L. Zhao, H. Liu, X. Jia, D. Mu, S. Liu, X. Dong, J. Zhang, W. Lu, G. Wang, Y. Zhou, Y. Zhu, X. Wang, Z. Xu, C. Chen, and X.J. Zhou, Nature **462**, 335 (2009).

[36] P.D.C. King, J.A. Rosen, W. Meevasana, A. Tamai, E. Rozbicki, R. Comin, G. Levy, D. Fournier, Y. Yoshida, H. Eisaki, K.M. Shen, N.J.C. Ingle, A. Damascelli, and F. Baumberger, Phys. Rev. Lett. **106**, 127005 (2011).

[37] E.A. Yelland, J. Singleton, C.H. Mielke, N. Harrison, F.F. Balakirev, B. Dabrowski, and J.R. Cooper, Phys. Rev. Lett. **100**, 047003 (2008).

[38] S.E. Sebastian, N. Harrison, E. Palm, T.P. Murphy, C.H. Mielke, R. Liang, D.A. Bonn, W.N. Hardy, and G.G. Lonzarich, Nature **454**, 200 (2008).

[39] D. LeBoeuf, N. Doiron-Leyraud, J. Levallois, R. Daou, J.-B. Bonnemaison, N.E. Hussey, L. Balicas, B.J. Ramshaw, R. Liang, D.A. Bonn, W.N. Hardy, S. Adachi, C. Proust, and L. Taillefer, Nature **450**, 533 (2007).

[40] J. Chang, Y. Sassa, S. Guerrero, M. Månsson, M. Shi, S. Pailhés, A. Bendounan, R. Mottl, T. Claesson, O. Tjernberg, L. Patthey, M. Ido, M. Oda, N. Momono, C. Mudry, and J. Mesot, New J. Phys. **10**, 103016 (2008).

[41] K. McElroy, D.-H. Lee, J.E. Hoffman, K.M. Lang, J. Lee, E.W. Hudson, H. Eisaki, S. Uchida, and J.C. Davis, Phys. Rev. Lett. **94**, 197005 (2005).

[42] W.D. Wise, M.C. Boyer, K. Chatterjee, T. Kondo, T. Takeuchi, H. Ikuta, Y. Wang, and E.W. Hudson, Nat. Phys. **4**, 696 (2008).

[43] M.C. Boyer, W.D. Wise, K. Chatterjee, M. Yi, T. Kondo, T. Takeuchi, H. Ikuta, and E.W. Hudson, Nat. Phys. **3**, 802 (2007).

[44] T.A. Webb, M.C. Boyer, Y. Yin, D. Chowdhury, Y. He, T. Kondo, T. Takeuchi, H. Ikuta, E.W. Hudson, J.E. Hoffman, and M.H. Hamidian, Phys. Rev. X **9**, 021021 (2019).

[45] Y. He, Y. Yin, M. Zech, A. Soumyanarayanan, M.M. Yee, T. Williams, M.C. Boyer, K. Chatterjee, W.D. Wise, I. Zeljkovic, T. Kondo, T. Takeuchi, H. Ikuta, P. Mistark, R.S. Markiewicz, A. Bansil, S. Sachdev, E.W. Hudson, and J.E. Hoffman, Science **344**, 608 (2014).

[46] A. Pushp, C.V. Parker, A.N. Pasupathy, K.K. Gomes, S. Ono, J. Wen, Z. Xu, G. Gu, and A. Yazdani, Science **324**, 1689 (2009).

[47] J. Lee, K. Fujita, A.R. Schmidt, C.K. Kim, H. Eisaki, S. Uchida, and J.C. Davis, Science **325**, 1099 (2009).

[48] U. Chatterjee, M. Shi, A. Kaminski, A. Kanigel, H.M. Fretwell, K. Terashima, T. Takahashi, S. Rosenkranz, Z.Z. Li, H. Raffy, A. Santander-Syro, K. Kadowaki, M.R. Norman, M. Randeria, and J.C. Campuzano, Phys. Rev. Lett. **96**, 107006 (2006).

[49] U. Chatterjee, M. Shi, A. Kaminski, A. Kanigel, H.M. Fretwell, K. Terashima, T. Takahashi, S. Rosenkranz, Z.Z. Li, H. Raffy, A. Santander-Syro, K. Kadowaki, M. Randeria, M.R. Norman, and J.C. Campuzano, Phys. Rev. B **76**, 012504 (2007).

[50] K. McElroy, G.-H. Gweon, S.Y. Zhou, J. Graf, S. Uchida, H. Eisaki, H. Takagi, T. Sasagawa, D.-H. Lee, and A. Lanzara, Phys. Rev. Lett. **96**, 067005 (2006).

[51] Q.-H. Wang and D.-H. Lee, Phys. Rev. B **67**, 020511 (2003).

[52] R.S. Markiewicz, Phys. Rev. B **69**, 214517 (2004).

[53] L. Capriotti, D.J. Scalapino, and R.D. Sedgewick, Phys. Rev. B **68**, 014508 (2003).

[54] Deheng Gao, Yingping Mou, Yiqun Liu, Shuning Tan, and Shiping Feng, Phil. Mag.**99**, 752-769 (2019).

[55] J.E. Hoffman, K. McElroy, D.-H. Lee, K.M. Lang, H. Eisaki, S. Uchida, and J.C. Davis, Science **297**, 1148 (2002).

[56] I.M. Vishik, E.A. Nowadnick, W.S. Lee, Z.X. Shen, B. Moritz, T.P. Devereaux, K. Tanaka, T. Sasagawa, and T. Fujii, Nat. Phys. **5**, 718 (2009).

[57] Shuning Tan, Yingping Mou, Yiqun Liu, and Shiping Feng, J. Supercond. Nov. Magn. **33**, 2305-2311 (2020)..

[58] M. Hashimoto, R.-H. He, J. P. Testaud, W. Meevasana, R. G. Moore, D. H. Lu, Y. Yoshida, H. Eisaki, T. P. Devereaux, Z. Hussain, and Z.-X. Shen, Phys. Rev. Lett. **106**, 167003.

[59] A. Kreisel, Peayush Choubey, T. Berlijn, W. Ku, B. M. Andersen, and P. J. Hirschfeld, Phys. Rev. Lett. **114**, 217002 (2015).

[60] J. W. Alldredge, E. M. Calleja, J. Dai, H Eisaki, S Uchida and K. McElroy, J. Phys.: Condens. Matter **25**, 33560 (2013).

[61] E. G Dalla Torre, Y. He, D. Benjamin, and E. Demler, New J. Phys. **17**, 022001 (2015).

[62] T. J. Reber, N. C. Plumb, Z. Sun, Y. Cao, Q. Wang, K. McElroy, H. Iwasawa, M. Arita, J. S. Wen, Z. J. Xu, G. Gu, Y. Yoshida, H. Eisaki, Y. Aiura and D. S. Dessau , Nat. Phys. **8**, 606-610 (2012).

[63] J.C. Campuzano, H. Ding, M.R. Norman, H.M. Fretwell, M. Randeria, A. Kaminski, J. Mesot, T. Takeuchi, T. Sato, T. Yokoya, T. Takahashi, T. Mochiku, K. Kadowaki, P. Guptasarma, D.G. Hinks, Z. Konstantinovic, Z.Z. Li, and H. Raffy, Phys. Rev. Lett. **83**, 3709 (1999).

[64] See Supplemental Material at *** for (a) an estimate of the impact of background subtraction from ARPES data on autocorrelation patterns and (b) the relation between the Fermi arc-length ($l(t)$) and $|\mathbf{q}_1|$ at ω=0 meV.